JOURNAL OF MATERIALS SCIENCE 19 (1984) 695–715

Review
Structure, properties and production of β-alumina

R. STEVENS, J. G. P. BINNER
Department of Ceramics, University of Leeds, Leeds, UK

The crystal structures of the β-alumina compositions have been described and used to explain the fast ion transport for which these materials are renowned. Measured values of both the single crystal and polycrystalline ionic conductivity show a wide variation; this is explained in terms of the range of chemical compositions of the β-alumina system and also the variety of measuring techniques used. Dopants or impurity ions can have a significant effect on the physical properties of the β-aluminas. The ionic conductivity, the stability of the material and the densification during sintering have been considered in relation to the nature and level of a range of dopants described in the literature. The optimization of the ionic and mechanical properties has been achieved by development of the fabrication techniques and it is this which accounts for much of the present research. Thus the many different methods of producing both single and polycrystalline material have been described, including the range of sintering routes currently available. The advantages and disadvantages of each production route in terms of the resulting properties have also been discussed.

1. Introduction

The β-aluminas possess an unusual layered crystal structure which permits extremely fast ion transport. The exploitation of this phenomenon presents a series of challenges to the materials scientist to achieve a balance of usable mechanical, electrical and electrochemical properties. One such application [1] is a secondary battery utilizing molten sodium as the anode and molten sulphur–sodium polysulphide as the cathode with β-alumina as a solid electrolyte. To obtain a higher conductivity for the cathode (sulphur being a poor conductor) it is impregnated into graphite felt.

The sodium–sulphur battery (Fig. 1) works on the principle of the ceramic electrolyte being impermeable to sodium metal and sulphur but permeable to sodium ions. When an external circuit is completed, Na^+ ions diffuse through the electrolyte producing sodium polysulphides as the discharge product, and electrons pass round the external circuit into the sulphur electrode producing an open circuit voltage of 2.08 V.

This battery was first conceived by Weber and Kummer [2] at the Scientific Laboratories of the Ford Motor Company in the early 1960s. A similar sodium–sulphur battery [3] was also devised at about the same time by Levine of the Dow Chemical Company. In this the electrolyte consists of bundles of thousands of special borate glass capillaries.

Despite this and alternative ceramic electrolyte candidates discovered recently, for example the three-dimensional conductor "Nasicon" ($Na_3Zr_2PSi_2O_{12}$) [4, 5], the β-aluminas are considered to be the preferred electrolytic material.

2. Crystal structure of β-alumina

In 1916 the existence of a new phase, which was believed to be a polymorph of α-Al_2O_3, and hence was termed β-Al_2O_3, was reported by Rankin and Merwin [6]. Ten years later, in 1926, Stillwell [7] recognized the need for the presence of soda in the production of this material, but still did not consider the soda to have an integral part in the final

0022–2461/84 $03.00 + .12

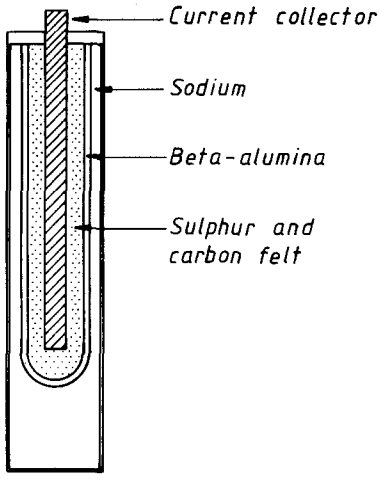

Figure 1 Schematic diagram of sodium–sulphur cell.

structure. This realization finally occurred when Bragg *et al.* [8] published the first crystal structure determination in 1931.

The structure was believed to consist of blocks, similar in construction to spinel, linked together by oxygen and alkali ions in loose-packed layers. The "spinel" blocks comprised four layers of oxygen ions in a cubic close-packed arrangement with the magnesium and aluminium "spinel" sites exclusively containing aluminium atoms. The sodium-containing layers also act as mirror planes for the close-packed oxygen layers on either side. Two views of the structure can be seen in Fig. 2.

However, the inaccuracy in the chemical analyses at that time caused Bragg *et al.* [8] to assume a composition which was inconsistent with the space-group symmetry, $P6_3/mmc$. This led them to suggest random positions for the alkali atoms in the loose-packed layers.

When, in 1936, a more exact formula for β-Al_2O_3 was ascertained, both from increased accuracy of chemical analysis [10] and from X-ray measurement of the unit cell and the density [11], the basic crystal structure suggested by Bragg *et al.* [8] was confirmed and the uncertainty in the mirror plane structure at least partially resolved. The work of Beevers and Ross [12] resulted, however, in there being two possible positions for the sodium atoms. These positions are at $(00\frac{1}{4})$ and $(\frac{2}{3}\frac{1}{3}\frac{1}{4})$ when the origin is taken at one of the centres of symmetry; $(\frac{2}{3}\frac{1}{3}\frac{1}{4})$ was considered more likely since the intensity fit for this position was substantially better. Felsche [13] was in agreement with this conclusion following his analysis of the structure using three-dimensional data, reporting that no electron density was observed at the position $(00\frac{1}{4})$. However, he also reported a deficiency of sodium and oxygen in the interlayer; only $\frac{1}{3}$ of the sodium sites suggested by Beevers and Ross [12] were occupied. Felsche [13] concluded that this was due to exchange of sodium ions by the hydroxyl H_3O^+ ion, with the composition $Na_2Al_{22}O_{34}$ being one limit in a series having $2HO \cdot Al_{22}O_{34}$ as the other extreme.

This work was subsequently criticized by Peters *et al.* [14] who considered the specimen crystal used by Felsche to be atypical. Instead, Peters *et al.* [14] believed that normal β-Al_2O_3 crystals contained an excess of about 15 to 30% soda [15] relative to the ideal formula and thus β-Al_2O_3 was, in fact, an off-stoichiometric, massively defective structure.

Yao and Kummer [15] believed that the stoichiometric sodium ions existed at the position $(\frac{2}{3}\frac{1}{3}\frac{1}{4})$, termed Beevers–Ross (BR) position by

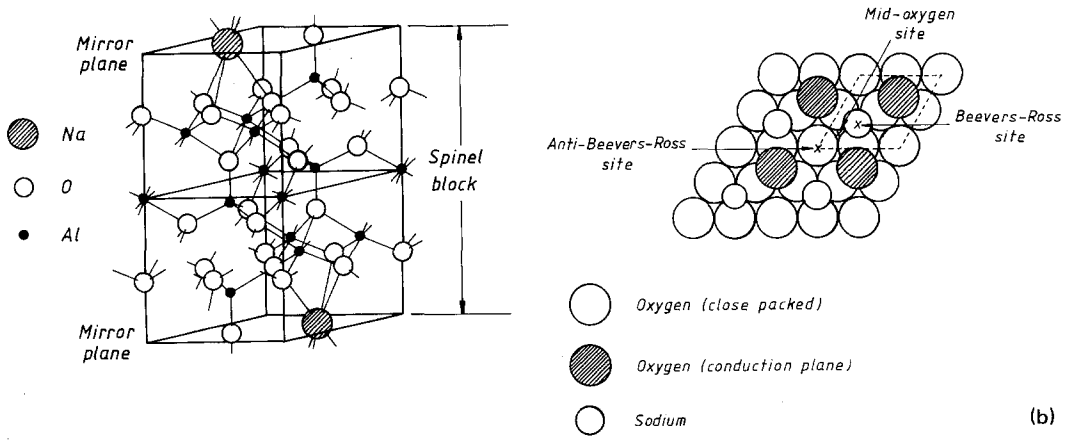

Figure 2 (a) Perspective diagram of half the unit cell. (b) Conduction plane of sodium β-alumina.

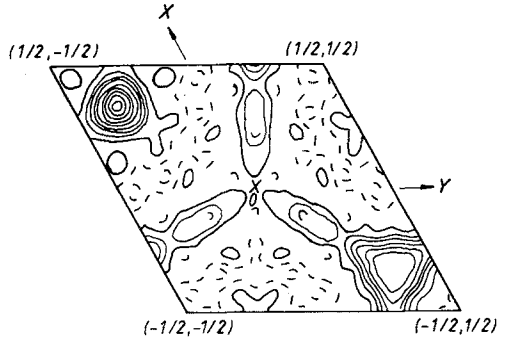

Figure 3 Fourier section showing electron density of β-alumina in mirror plane at $z = 1$.

Peters *et al.* [14], whereas the excess ions existed at the position $(00\frac{1}{4})$, termed anti-Beevers–Ross (aBR). The Fourier section at $z = \frac{1}{4}$ (Fig. 3) deduced by Peters *et al.* [14] indicated a broad and triangular high electron density at the BR position and nothing at the aBR position. It also showed a smaller electron density in a new, hitherto unconsidered position. This was at $(\frac{5}{6}\frac{1}{6}\frac{1}{4})$, the mid-point between linking oxygens in the loose-packed layer and hence was referred to as the mid-oxygen (mO) position. The three sites BR, aBR and mO are shown in Fig. 2b.

The mO position has six-fold coordination and was not considered by Beevers and Ross [12] who were looking only at twofold positions. A least-squares analytical method indicated that a greater proportion of the sodium atoms (1.51 atoms per site per unit cell) existed near the BR position then the mO position (1.06 atoms per site per unit cell). However, Peters *et al.* [14] also reported that only about 75% of the BR positions were occupied.

On account of the sodium ion concentration being greater than that required for the ideal crystal structure, the existence of counter-ion defects was considered to balance the excess positive charge. Such defects were used by Peters *et al.* [14] to explain both the triangular distortion of the electron density and the 75% level of occupancy of the BR sites. The defect suggested was aluminium ion vacancies, the electric fields of which, it was suggested, would tend to completely dislodge the closest sodium ions in BR positions and distort the electron density of those remaining.

Later, neutron diffraction studies [16] showed that the overall positive charge accruing from the excess Na^+ ions was actually balanced by interstitial oxygen ions in the conduction plane, these latter being pinned by Frenkel defects to the aluminium ions in the "spinel" blocks. The result is a linear defect which can be represented by:

$$V_{Al}Al_i - O_i^{2-} - Al_iV_{Al}$$

where $V_{A1}Al_i$ describes the Frenkel defect connected through an interstitial oxygen ion in the loose-packed plane to its mirror image in the next "spinel" block.

Recently, nuclear magnetic resonance studies [17] have suggested that for β-Al_2O_3 compositions very rich in sodium, further new sites are inhabited by sodium ions. Ion exchange experiments [18] indicate that these sites may be such that the sodium ions are not mobile. The maximum soda content possible in β-Al_2O_3 appears to be close to the composition $(Na_2O)_{1+x}\cdot 11Al_2O_3$ where $x \approx 1$, in reasonable agreement with the phase diagram (see Section 3).

The existence of a second compound in the $Na_2O\cdot Al_2O_3$ system was first reported in 1943 by Yamaguchi [19]. It was found to have an X-ray diffraction pattern similar to that of β-Al_2O_3 but could not be properly indexed unless a c-axis 1.5 times as long was assumed. Just over 10 years later Yamaguchi re-investigated this material and discovered not one but two new phases with approximate compositions $Na_2O\cdot 8.1Al_2O_3$ and $Na_2O\cdot 5.18Al_2O_3$ which he named β' and β'' Al_2O_3 respectively. The structure of the β' phase was found to be similar to that of the β phase whilst that of the β'' phase involved cubic close-packing of the oxygen ions with alkali-bearing layers dispersed at intervals, but the latter did not act as mirror planes for the close-packed oxygen layers.

Unaware of this work, Théry and Briançon [20, 21] also reported the existence of a new compound with formula $Na_2O\cdot 5Al_2O_3$. They also discovered that a second compound, $Na_2O\cdot 7.02Al_2O_3$, was formed by prolonged heating of the first at 1350° C.

The crystal structure of β''-Al_2O_3 ($Na_2O\cdot 5Al_2O_3$) was first determined by Yamaguchi and Suzuki [22] in 1968 by using only X-ray powder diffraction data. It was found to be rhombohedral with space group $R\bar{3}m$ and a c-axis of 3.395 nm (cf. 2.245 nm for β-Al_2O_3). The unit cell of β-Al_2O_3 consists of two 1.123 nm "spinel" blocks related by a two-fold screw axis parallel to the c-axis, whereas that of β''-Al_2O_3 comprises three 1.123 nm "spinel" blocks related by a three-fold screw axis. Just as in β-Al_2O_3 the blocks are linked by Al–O–Al bonds with all the Na^+ ions stituated

in these loose-packed layers, this giving rise to the high ionic conductivity for which these materials are noted (see Section 4). Owing to the three-fold screw axis the sodium-containing layer does not act as a mirror plane for the two oxygen layers above and below it. Instead these oxygen planes are staggered resulting in a different geometry for the Na^+ ions.

In the BR position in β-Al_2O_3, the sodium ions occupy the centre of triangular prisms of six oxygen atoms (O–Na distance is 0.287 nm). However, when travelling through the conduction layer the sodium ions must pass through the aBR positions, i.e. between 2 oxygen atoms 0.238 nm apart. Na^+ (ionic diameter 0.190 nm) is small enough to pass through this gap, but K^+ (ionic diameter 0.266 nm) and the larger alkali ions are too large to pass through with ease.

The geometry of the β''-Al_2O_3 conduction plane presents no such problem. Owing to the staggering of the layers all the sodium ions occupy the centre of a tetrahedron of oxygen atoms, the apex being 0.257 nm away and the triangular base oxygens 0.269 nm from the central Na^+ ion. Each unit cell contains two such positions on each conduction plane, one the invert of the other. A view of the structure compared to that of β-alumina can be seen in Fig. 4.

In agreement with Kummer [23] it is believed that β'-Al_2O_3 is simply β-Al_2O_3 containing the usual excess of Na_2O, since there are no reports other than that by Yamaguchi [19] in the literature concerning this material.

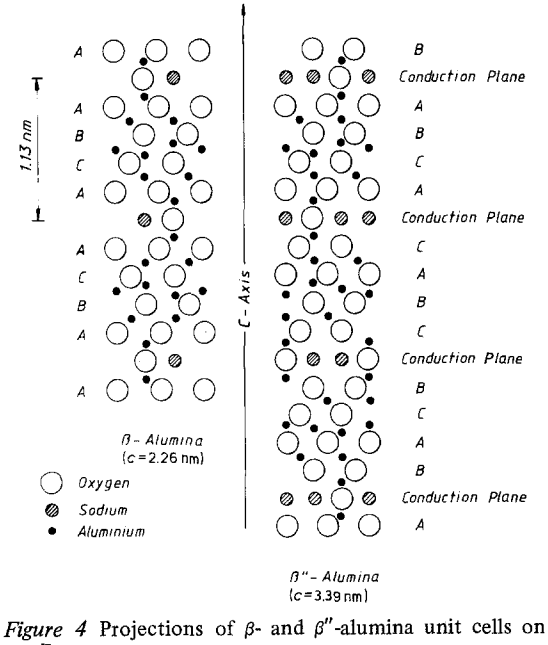

Figure 4 Projections of β- and β''-alumina unit cells on $(11\bar{2}0)$.

Two other β-alumina compounds (β-alumina being a generic as well as a specific name) have been named [24], β'''-Al_2O_3 and β''''-Al_2O_3. The former has a structure similar to β-Al_2O_3 (i.e. 2 block); however the spinel block is 1.59 nm thick rather than 1.13 nm since it contains six close-packed oxygen layers instead of the usual four ($a = 0.562$ nm, $c = 3.18$ nm). β''''-Al_2O_3 bears the same structural relationship to β'''-Al_2O_3 as β''-Al_2O_3 does to β-Al_2O_3, i.e. it is three-block with each spinel block 1.59 nm thick. These compounds have been found in the ternary system Na_2O–MgO–Al_2O_3 and not in binary Na_2O–Al_2O_3.

3. Phase relationships in the β-alumina system

The phase diagram for the $NaAlO_2$–Al_2O_3 system has yet to be defined exactly. In 1965 Rolin and Thank [25] determined liquidus curves directly using molybdenum crucibles and an argon atmosphere. Soda loss was minimized by using large samples and reaction of the melt with the molybdenum was considered negligible.

These curves were considered to be essentially correct from the eutectic point to the high-alumina end of the diagram by De Vries and Roth [26] in their review of the literature in 1969. They proposed that the β'' phase existed over the composition range $Na_2O{\cdot}5.33Al_2O_3$ to $Na_2O{\cdot}7Al_2O_3$ (i.e. soda deficient) and to dissociate at 1550° C to β-Al_2O_3 and δ-$NaAlO_2$; above 1550° C only the β phase was stable and this was invariably soda-rich with respect to the formula $Na_2O{\cdot}11Al_2O_3$. However, at temperatures below 1550° C they were unable to decide whether β-Al_2O_3 was stable or metastable with respect to β''. They constructed therefore, two feasible phase diagrams, corresponding to the two cases. Subsequently, Liebertz [27] investigated this uncertainty and found that both β and β'' phases existed between 85 and 90 mol% Al_2O_3, with the β phase stable above 1550° C and the β'' phase stable below this temperature.

Le Cars *et al.* [28, 29] concluded that whilst the β'' to β transformation was complete above 1550° C, it was not reversible on cooling, and that it was the β phase which was stable below 1550° C, the β'' phase being metastable at all temperatures

in the pure binary system. The system has a eutectic between β-alumina and δ-$NaAlO_2$ melting at 1585° C and a peritectic between β-alumina and α-alumina at ~2000° C. β″ is suggested as being metastable above 1585° C and that β and β″ coexist at temperatures below this, where β may be metastable. Evidence for this latter case is that β″-alumina is formed if Na_2O is evaporated from $NaAlO_2$ at 950° C [29]. Bevan *et al.* [30] have shown that β-alumina forms disordered intergrowth structures consisting of β- and β″-alumina which may explain the failure of Le Cars *et al.* [28, 29] to observe independent β and β″ phases.

Nevertheless the question as to whether β″-alumina is metastable in the Na_2O–Al_2O_3 system is not of great practical importance as the phase is normally produced in the presence of additions of MgO or Li_2O which help stabilize it, even at temperatures as high as 1700° C [31].

A phase diagram of the MgO–Na_2O–Al_2O_3 system in the high Al_2O_3 range was obtained by Weber and Verero [32] and the equilibrium subsolidus relations at 1700° C are shown in Fig. 5. In addition to β and β″, phases designated β‴ and β⁗ were identified. The crystal structures of these were outlined at the end of Section 2.

A preliminary study of the Li_2O–Na_2O–Al_2O_3 system has been reported [33] and the principal features of the Al_2O_3-rich portion of this system are shown in Fig. 6. There is a pseudo-binary eutectic between $NaAlO_2$ and $LiAlO_2$ and a pseudo-ternary eutectic between $NaAlO_2$, $LiAlO_2$ and β″-alumina. So far a methodical study of the Li_2O–MgO–Na_2O–Al_2O_3 system has yet to be reported.

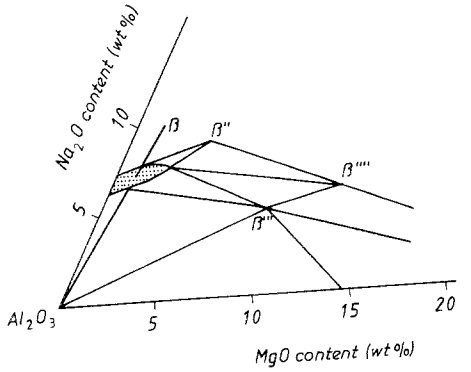

Figure 5 Equilibrium subsolidus relations in the high Al_2O_3 area of the $NaAlO_2$–$MgAl_2O_4$–Al_2O_3 system at 1700° C.

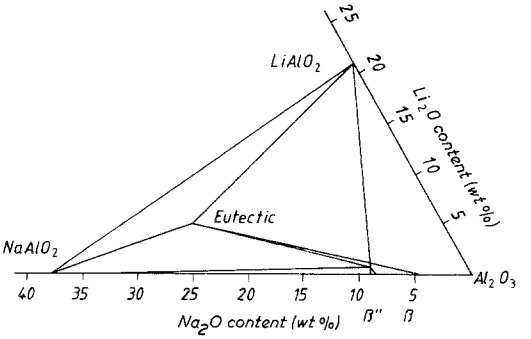

Figure 6 Phase relations in the high alumina area of the Al_2O_3–$NaAlO_2$–$LiAlO_2$ system.

4. Conductivity of β-Al_2O_3

4.1. Single crystal conductivity

The structure of the β-aluminas (see Section 2) results in Na^+ ions being able to move freely in the loose-packed layer under the application of an applied electric field, i.e. the β-alumina compositions are Na^+-ion conductors. This was first reported by Saalfield [34] in 1956. Using molten salts (300 to 350° C) the ion exchange ability of the Na^+ ions in β-alumina was determined with respect to other monovalent ions.

The occurrence of this ion exchange indicated that the monovalent ions in the loose-packed planes were mobile and should, therefore, possess high diffusion coefficients. The self-diffusion coefficients for Na^+, K^+, Rb^+ and Ag^+ in β-alumina crystals were therefore measured by Yao and Kummer [15] using radioactive isotopes of the above ions. They also obtained values for Li^+ using a stable isotope and neutron irradiation, forming ^{18}F which was analysed quantitatively. These values are shown in Table I, together with values for Tl^+ obtained by Radzilowski [36], and Na^+ in polycrystalline β-alumina by Dunbar and Sarian [37].

The method employed by Yao and Kummer [15] also illustrated the high anisotropy expected of this material from its crystal structure. The radioactive isotope ^{24}Na was produced by neutron irradiation; however, on formation, the excited ^{24}Na instantaneously emits a gamma ray and the recoil energy is sufficient to drive some of the ions into the "spinel" blocks. These ions could only be recovered by an anneal at 1100° C for half an hour, despite the fact that the maximum distance they had to travel was ~0.6 nm. Demott and Hancock [38] have also shown that the conductivity perpendicular to the *c*-axis is much larger than that parallel to it, by a factor of 100 to 1000.

TABLE I Comparison of activation energies for tracer diffusion with activation energies for conductivity (single crystal samples)

Ion	D_0 ($cm^2 sec^{-1}$)	$E_{act.}$ (kcal mol^{-1})		Calculated D_t (25° C) ($cm^2 sec^{-1}$)	$\sigma_{25°C}$ (Ω^{-1}-cm^{-1})	Calculated D_σ (25° C) ($cm^2 sec^{-1}$)	D_t/D_σ
		D	σ				
Na^+	2.4×10^{-4}	3.81	3.78	4.0×10^{-7}	140×10^{-4}	6.8×10^{-7}	0.59
Na^{+*}	2.0×10^{-4}	3.60	–	5.0×10^{-7}	–	–	–
Ag^+	1.65×10^{-4}	4.05	3.98	1.7×10^{-7}	64×10^{-4}	3.1×10^{-7}	0.55
K^+	0.78×10^{-4}	5.36	6.78	9.6×10^{-9}	0.65×10^{-4}	3.17×10^{-9}	3.0
Rb^+	0.34×10^{-4}	7.18	–	1.9×10^{-10}	–	–	–
Tl^+	0.65×10^{-4}	8.22	8.19	6.2×10^{-11}	0.02×10^{-4}	9.76×10^{-11}	0.63
Li^+	14.5×10^{-4}	8.71	$8.45^{high\ temp.}$ $4.30^{low\ temp.}$	–	1.3×10^{-4}	–	–

*Hot-pressed polycrystalline sample.

Accompanying the self-diffusion coefficients in Table I is a comparison of the activation energies for tracer diffusion with those for conductivity, obtained using single crystals. The close agreement between these values indicates that the mechanism for these two transport processes must be the same.

As a result of the different crystal structures of β- and β''-alumina and, in particular, the different geometry of the Na^+ ion sites, the two materials have different conductivities. Hooper [39] has reported resistivity values of 4.7 Ω cm for β-Al_2O_3 and 1 Ω cm for β''-Al_2O_3 at 300° C. The lower value of β''-Al_2O_3 is due to the more favourable structure of the conduction planes, and thus the resulting lower activation energy for conduction. However, a degree of variation exists in the reported values for the resistivities of the sodium β-aluminas. For example, for β-Al_2O_3, Imai and Harata [33] obtained a room temperature value of 30.303 Ω cm (after extrapolation and using reversible molten sodium electrodes), whereas Whittingham and Huggins [40] quote the room temperature value as 71.429 Ω cm (using tungsten bronze electrodes, Na_xWO_3, which exhibit both ionic and electronic conductivity and function as a reversible sodium electrode in cells of the type Na_xWO_3/β-Al_2O_3/Na_xWO_3). It is not known, however, whether this difference in result occurs because of the different measuring techniques or different sample composition, since it has been found that the conductivity is sensitive to sodium content [41].

4.2. Conduction mechanism

The variation in conductivity with sodium content can be anticipated from consideration of the structure of the conduction plane. It has been found [42] that the conductivity of a single crystal, composition $(Na_2O)_2 \cdot 11Al_2O_3$, is an order of magnitude less than for the normal, nonstoichiometric composition $((Na_2O)_{1+x} \cdot 11Al_2O_3$ where $x = 0.2$ to 0.3). The activation energy for conductivity also varies. It is far greater at both high [42] and low [43] stoichiometric limits. This is shown in Fig. 7.

In 1973 Le Cars *et al.* [44] reported the existence of an order–disorder phenomenon involving the atoms in the conduction plane. Unlike other superionic conductors, e.g. AgI or $RbAg_4I_5$, there was no discrete transition temperature, but a gradual tendency towards a disordered structure with increasing temperature. Using Raman spectroscopy and the actual stoichiometric compound, $Na_2O \cdot 11Al_2O_3$, Colomban and Lucazeau [45] confirmed the existence of an ordered state at low temperatures, finding that dynamic cation disorder started to occcur with temperatures in excess of ~100 K for the sodium form and ~350 K for the silver form. They concluded, therefore, that stoichiometric β-alumina could be considered as a superionic conductor above these characteristic temperatures.

Studies of the transport properties of Na^+ and Ag^+ β-alumina [40, 46] led Whittingham and Huggins to calculate for both materials a value of ~0.60, for the ratio D_t/D_σ, where D_t is the tracer diffusion coefficient and D_σ is the diffusion coefficient from the electrical conductivity (this ratio being termed the Haven ratio, H_R). Such a value led them to discount an interstitial mechanism for monovalent ion diffusion in β-alumina. Instead Whittingham and Huggins [46] suggested an interstitialcy mechanism. This latter mechanism was first defined by Koch and Wagner [47] in 1937 and is the movement of an ion residing in an inter-

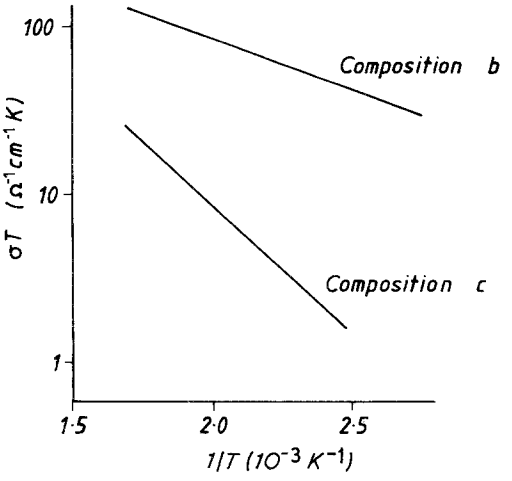

Figure 7 Ionic conductivity of soda-rich β-alumina.

Activation energies of ionic conductivity

Composition	Na content (wt %)	$E_{act.}$ (eV)
a. $(Na_2O)_{1.00}\cdot 11Al_2O_3$	4.04	0.62
b. $(Na_2O)_{1.25}\cdot 11Al_2O_3$	5.03	0.13
c. $(Na_2O)_{2.00}\cdot 11Al_2O_3$	7.97	0.30

stitial site into a regular lattice site, displacing the ion there to another neighbouring interstitial site. This interstitialcy mechanism therefore assumes the use of Beevers–Ross (regular lattice) and anti-Beevers–Ross (interstitial) sites and so fails to explain the existence of about one-third of the Na^+ ions at mid-oxygen positions.

Wang *et al.* [48] suggested a similar mechanism which involved mO–mO interstitialcy configurations combined with the regular lattice BR positions. Using this model they constructed potential energy curves for the path of the mobile ion from BR site to aBR site. In addition they calculated activation energies with first two and then six M^+ ions allowed to adjust their positions to minimize the total potential energy. The calculated values assuming adjustment of six M^+ ions compared favourably with experimental values for activation energy and the mechanism also agreed well with the observed occupation of mO and BR cation sites [14]. However, their mechanism fails to account satisfactorily for the small, but finite, observed occupation of the aBR sites [16] in Na β-Al_2O_3 and much larger occupancy in Ag β-Al_2O_3 [49].

Wolf [50] has criticized the previous two mechanisms for a variety of reasons. These included (i) the lack of agreement with observed occupancy levels of the three mobile ion sites, (ii) the omission of the effects associated with the presence of oxygen ion interstitials, O_i^{2-}, which have been reported by Roth *et al.* [16], and, more recently, McWhan *et al.* [51]; (iii) the calculated value of H_R by Whittingham and Huggins [46] was not in agreement with the later experimental values of Kim *et al.* [51]; and (iv) the mechanisms did not suggest an explanation for the observation that spectroscopic diffusion techniques yielded more than one activation energy. The techniques seemed to study more than one type of motion while, in the same temperature range, transport techniques revealed a unique value of the activation energy.

The theory proposed by Wolf [50] attempts to account for all the above factors. In Wolf's mechanism the ions move in pairs as for the previous two mechanisms, but all three cation sites are now involved. Fig. 8a shows sodium ions existing at the BR sites (marked 1) with one extra ion at an aBR site (marked 2). The "interstitial" ion then jumps, together with a "regular lattice" ion into a position such as that seen in Fig. 8b. The two ions thus occupy an mO–mO configuration (marked by 3's). The second step is a return to a BR–aBR configuration; this could be the original positions as in Fig. 8a or new positions, as in Fig. 8c, there being a probability of 0.5 for both of these options. Fig. 8d indicates that the "interstitial" ion then jumps again, either with a fresh

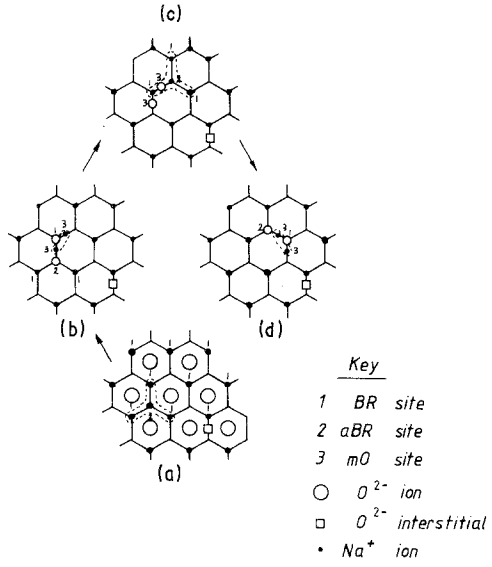

Figure 8 Interstialcy mechanism in the conduction plane of sodium β-alumina.

"regular lattice" ion or the original ion. Thus movement of the Na^+ ions occurs by the paired jumping of the ions using two equilibrium configurations and all three cation sites. Calculations of the resultant cation distributions on the three types of site for this mechanism are in good agreement with those determined experimentally [16]. Oxygen ion interstitials, discovered by Roth *et al.* [16], were believed to result in the "binding" of the excess Na^+ ions into "associated regions" around the charge-compensating oxygen ion. The Haven ratio was determined for various sizes of these associated regions and in agreement with the experimental measurements of Kim *et al.* [52], H_R was found to increase with increasing temperature as a result of the decrease in the average size of the associated regions. It was concluded that, while at lower temperatures all excess Na^+ ions were found in the regions around the oxygen interstitials, with increasing temperatures more and more of them were freely mobile in the unassociated regions of the conduction plane. This conclusion is in agreement with the results determined by Le Cars *et al.* [44] discussed earlier in this section.

Further supporting evidence for this mechanism comes from the Raman scattering results of Chase *et al.* [53]; they obtained two well-defined Raman peaks for Na β-Al_2O_3 at the frequencies $1.8 \times 10^{12}\,sec^{-1}$ and $3 \times 10^{12}\,sec^{-1}$. Wolf [50] calculated values for the attempt frequencies of the interstitialcy jumps and obtained the results: $(1.7 \pm 0.2) \times 10^{12}\,sec^{-1}$ and $(2.8 \pm 0.3) \times 10^{12}\,sec^{-1}$ for the mO–mO → aBR–BR and aBR–BR → mO–mO type jumps respectively. These results show extremely close agreement. Wolf's mechanism [50] results in two different regions in which an average Na^+ can be found. These are (i) trapped in one of the "associated regions", or (ii) fully mobile in an unassociated area of the conduction plane. In the first instance, the interstitialcy diffusion process will result in strongly localized motion, whereas in the second, long-range transport of mass and charge will occur. Both kinds of motion are detectable by spectroscopic techniques, whereas transport techniques, by their very nature, will only register the overall net movement of the ions, i.e. of the diffusion occurring outside the associated regions. This, therefore, explains the observation that spectroscopic techniques indicate two types of motion whilst transport techniques reveal only one.

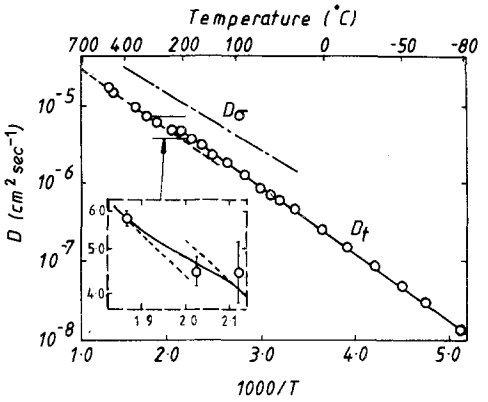

Figure 9 Sodium tracer diffusion in single-crystal sodium β-alumina. Values of D_σ calculated from the measured conductivity are included for comparison.

Whilst this theory appears to explain many of the experimental observations it is probably not entirely accurate. The data obtained by Kim *et al.* [52] for the variation in Haven ratio with temperature appears to indicate that the sodium diffusivity obeys two Arrhenius relations in the temperature range 0 to 600° C, one below 200° C and the other above 280° C, with a gradual changeover in the interval (Fig. 9). Such a discontinuity has never been reported for a plot of conductivity against temperature which, together with its small size, would indicate that it might be due to minor experimental artifacts. Kim *et al.* have suggested that the break may be due to some small structural transformation, in which case they expected to find evidence of a change in the lattice parameters as a function of temperature. X-ray diffraction measurements (in the *c*-direction only) did not detect any such change.

Owing to the small size of the discontinuity in

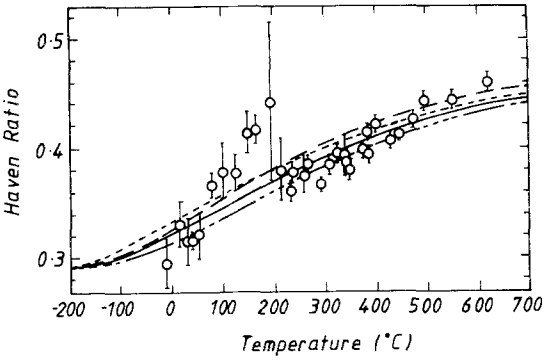

Figure 10 Comparison of the variation in Haven ratio as a function of temperature with the curves predicted by Wolf's mechanism.

the diffusivity measurements (Fig. 9) and lack of confirmation by all experimental techniques, both Kim *et al.* [52] and Wolf [50] have chosen to ignore its presence. Fig. 10, however, shows the magnitude of the effect of the discontinuity on the Haven ratio as a function of temperature and the lack of agreement with the curves predicted by Wolf's mechanism which results.

4.3. Polycrystalline conductivity

There are five principal factors which influence the conductivity of polycrystalline β-alumina. These are:

1. the relative proportion of β and β″ phases present;
2. the microstructure (grain size);
3. the proximity to theoretical density;
4. the presence of dopants (impurities);
5. the existence of basal plane defects.

The properties of polycrystalline ceramics are very dependent upon sintering conditions, and β-alumina is no exception. Fig. 11 shows the effect of firing temperature on the proportion of β- and β″-alumina. It can be seen how the fraction of β″-alumina decreases with firing temperature. The larger single crystal conductivity of β″-alumina over β-alumina described in Section 4.1 leads to a comparable difference in the polycrystalline resistivity. Typical values for the latter are those of May [54], these being 12.048 and 5.000 Ω cm, for β- and β″-alumina respectively at 300° C. Youngblood *et al.* [55, 56] reported that incomplete conversion to the β″-phase during sintering has a dominant influence on the ionic resistivity and its temperature dependence. Fig. 12 shows an approximately linear relationship between the resistivity and proportion of the two phases

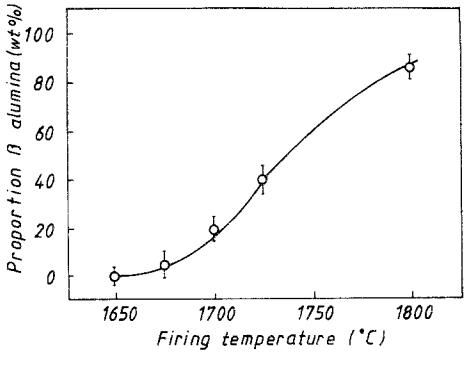

Figure 11 Variation of phase composition (β and β″) with zone sintering temperature for composition 8 wt % Na_2O 2 wt % MgO, 0.3 wt % Li_2O.

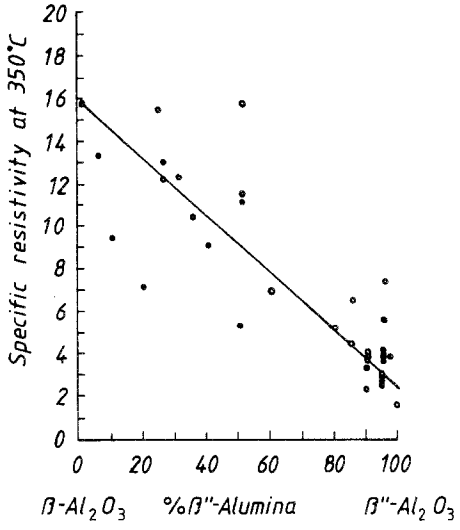

Figure 12 Resistivity of β-alumina as a function of β/β″ ratio.

present; the scatter of points arising from variations in density and microstructure of the samples.

The microstructure developed in β-alumina ceramics is very dependent upon the sintering temperature and time [56–59]. Higher temperatures or extended sintering times create a duplex structure in the form of large, unconnected lath shaped grains, ~200 μm x 20 μm, in a matrix of fine grains. Fig. 13a shows a typical fine grain structure and Fig. 13b indicates the appearance of discontinuous grain growth with firing temperature (using zone sintering and hence a short, ~1 min, and constant firing time).

Owing to the two-dimensional nature of the conduction planes in β-alumina the effect of grain size, and hence tortuosity, on conductivity is substantial. A decrease in conductivity by a factor of $\frac{2}{3}$ has been calculated for a totally randomly orientated sample [35]. However, this value may be somewhat different for practical ceramics where the fabrication route in some cases is found to influence the orientation considerably [60, 61] (e.g. the non-conductive *c*-axis can be orientated in a radial direction for electrolyte tubing). Ohta *et al.* [60] and Youngblood and Gordon [61] found differences in conductivity of 1.5 and 1.25 respectively in perpendicular directions in their samples. Youngblood *et al.* [56] found that the resistivity increased from 2.84 to 4.45 Ω cm as the grain size decreased from ~100 to 2 μm. Whalen *et al.* [58] performed similar experiments and their results are shown in Fig. 14. A strength of

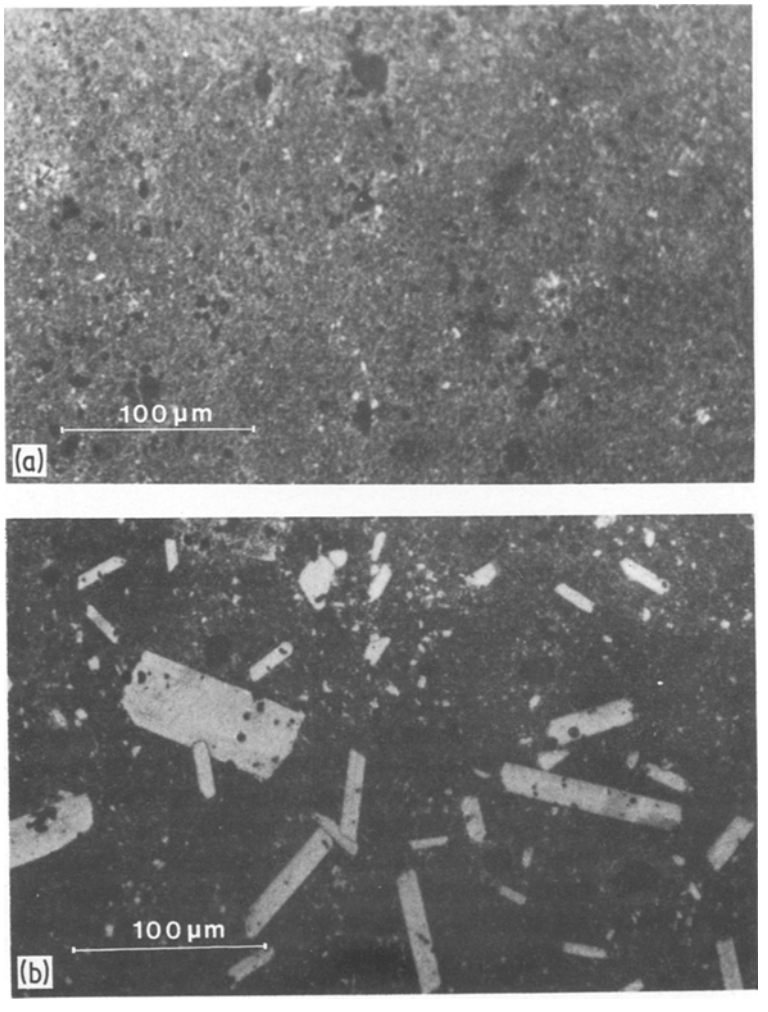

Figure 13 (a) Zone sintered at 1650° C. (b) Zone sintered at 1750° C, showing increased fraction of coarse grains and zone enclosed porosity within the large grains.

$\sim 193\,MN\,m^{-2}$ was measured with fine grain sizes ($\sim 3\,\mu m$) and also a resistivity of 9 to $10\,\Omega$ cm. Longer sintering times resulted in a coarser microstructure and reduced the resistivity by a factor of ~ 2, but also decreased the strength by a similar degree.

Fig. 15 shows the variation in density with firing temperature. The influence of this parameter on conductivity is relatively severe. Unless ceramic β-alumina is sintered to nearly theoretical density ($\sim 3.26\,g\,cm^{-3}$ depending upon composition), the conductivity is extremely low [35].

The effects of many different dopants on the properties of the β-aluminas have been investigated; their influences are described in Section 5.

It has already been shown in Section 4.1 that Na^+ ion conduction normal to the spinel blocks is several orders of magnitude slower than in the loose-packed conduction plane [15, 38]. This high anisotropy presents special problems for ion conduction in polycrystalline or defect-containing electrolyte. Basal plane defects such as dislocations, stacking sequence faults, intergrowth and low-angle tilt boundaries have all been found in β-alumina grains [62–65]. Conduction only occurs to any appreciable extent along the basal plane [62, 66], hence it is possible that these faults will affect the rapid homogeneous flow of sodium ions during d.c. conduction by causing the sodium ions to take a more tortuous route by blocking their path, thereby increasing the resultant resistivity [67].

4.4. Measurement of conductivity

The measurement of conductivity can be accomplished by one of two basic approaches when dealing with solid electrolytes. The first, and most straight-forward conceptually, is to use a d.c. signal with reversible electrodes, the resistance being calculated from Ohm's law. However, for

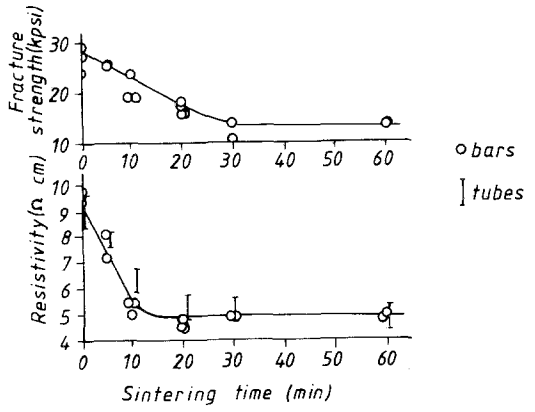

Figure 14 Various physical parameters as functions of sintering time.

Various physical parameters as functions of sintering time

Sintering time (min)	Fine-grained fraction		Coarse-grained fraction	
	Average size (μm)	Distribution by area (%)	Average size (μm)	Distribution by area (%)
0	3	100		0
5	3	90	20	10
10	3	65	22	35
20	3	40	92	60
30	3	20	150	80
60	3	10	150	90

β-alumina, with measurements occurring in the range 300 to 350° C, the electrodes have to be either a fused sodium salt or metallic sodium, both of which cause handling problems. Also, whilst the use of four point d.c. measurements avoids polarization effects, it introduces restrictions on specimen geometry, the specimen having to be in the form of bars.

The second approach is to use irreversible electrodes and an a.c. signal which circumvents all the above problems. This approach also allows the possibility of the various capacitance effects being separated from the electrolytic resistance, using the frequency dependence of the conductivity. One particularly important result which can be obtained by this separation is the contribution made to the overall specimen resistance by the grain boundaries in a polycrystalline sample.

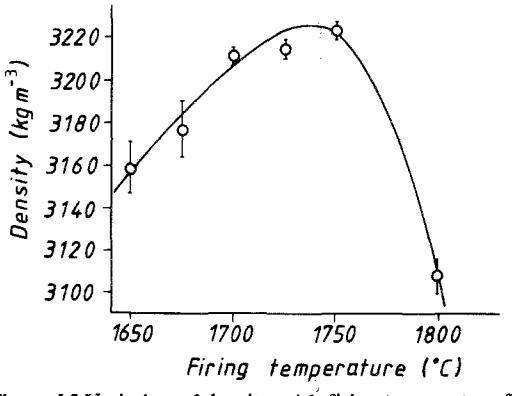

Figure 15 Variation of density with firing temperature for β-alumina.

5. Effect of dopants on β-alumina

The addition of dopants to the β-alumina system may vary the physical properties of the parent material for a variety of reasons, the nature of the dopant determining the role that is played. There are five roles which are usually considered [68], these being:

1. Certain metal cations which are able to exchange with the Na^+ ions in the conduction plane and therefore affect the conductivity because of their different diffusion coefficients.

2. The addition of cations which replace the Al^{3+} ions in the spinel blocks, thereby resulting in a charge imbalance; this will determine the concentration of mobile Na^+ ions in the conduction planes.

3. The relative stabilities of β- and β″-alumina are dependent upon the presence of certain dopants.

4. Other additives which will affect the degree of densification of the β-alumina, and hence the resistivity and strength.

5. The possibility of producing analogous compounds to β-alumina with other trivalent cations rather than Al^{3+}, these naturally having different properties.

Of these five roles the first has already been discussed in Section 4.1, and the last does not lie within the scope of the present work. The remaining three roles are discussed in the following sections.

5.1. Effect of additives on the concentration of conductive Na^+ ions

If an aluminium ion in the spinel block is replaced by a cation of lower charge then a deficit of positive charge will result. This imbalance may be overcome by either incorporating (i) a greater number of sodium ions or (ii) a lower number of oxygen interstitials in the conduction plane, or by reducing the number of aluminium vacancies in the spinel block. The relative degree of

importance of each of these mechanisms is as yet uncertain.

The variation of conductivity with sodium content has already been described in Section 4.2 and an explanation attempted. Kennedy and Sammells [69] studied the relationship between sodium content (and therefore conductivity) and magnesia doping level. The optimum sodium concentration was found to be dependent upon magnesia doping level, in that as the magnesia content increased so did the optimum sodium content. The results were consistent with the belief that for every Mg^+ added one extra Na^+ was incorporated compared to the undoped material.

Experiments have also been carried out [70] using other divalent cations; however the resulting increase in conductivity was much smaller than with magnesia doping.

5.2. Effect of additives on the stability of β''-Al_2O_3

It has been found [31, 71] that the cations which stabilize the β'' structure are those which are capable of occupying either the octahedral or tetrahedral sites in the spinel lattice. Boilot and Thery [71] determined that the critical ionic radius was 0.97 nm, thus Mg^{2+}, Ni^{2+}, Co^{2+}, Cu^{2+}, Zn^{2+}, Mn^{2+} and Cd^{2+} are all capable of stabilizing the β'' structure. The larger Pb^{2+}, Ca^{2+}, Sr^{2+} and Ba^{2+} are incapable of entering the spinel block, and as they tend to form the magnetoplumbite structure in the corresponding ferrite systems, are found not to stabilize the β''-Al_2O_3 phase but to favour the β-Al_2O_3. All the divalent cations of size <0.097 nm are transition metals, of potentially variable valency except for Mg^{2+}; it is for this reason that MgO and Li_2O are the preferred additives to β-Al_2O_3 for high ionic conductivity, with no electronic contribution.

Li^+ is regarded as being the most effective dopant with respect to stabilization of the β'' structure [72]. Magnesium forms a "normal" spinel, occupying the tetrahedral "A" sites as in the case of $MgAl_2O_4$. This results in the Mg^{2+} substituting for the Al^{3+} in the sites next to the conduction plane, which is not electrostatically favourable. It is suggested [72] that this may explain the hydration behaviour of 3 to 4 wt % MgO doped compositions [73] which suffer a loss in strength owing to an expansion in the *c*-axis of the unit cell.

Lithia, however, forms an inverse spinel with alumina ($LiAl_5O_8$), and hence the Li^+ are substituted for the octahedrally coordinated Al^{3+} ions in the centre of the spinel blocks. This is more electrostatically favourable and thus enhances the β'' structure to a greater degree.

It has been suggested [72] that stabilization occurs on account of the filling of cation vacancies. The substitutions $3Mg^{2+}$ for Al^{3+} and $3Li^+$ for Al^{3+} result in the same number of Mg^{2+} and Li^+ ions but with the former, one vacancy is filled whereas with Li^+ two vacancies are filled. A greater dopant addition (typically $\sim 3.8\%$) is therefore required with the former than the latter (typically $\sim 0.7\%$).

The function of additives in stabilizing one β-alumina phase or another depends upon their incorporation into the structure at the sintering stage [41]. A structural study [74] has shown that if lithium is inserted into the β-Al_2O_3 structure at a later stage, by ion exchange, then it is accommodated in the conduction planes rather than in the spinel block and does not cause the formation of β''-Al_2O_3.

Despite β''-Al_2O_3 being Na^+ deficient it has a higher conductivity by a factor of 3 to 5 over β-Al_2O_3 because of a higher concentration of mobile Na^+ ions. It can be concluded, however, that the dopants are not required for the purpose of charge compensation with respect to the sodium content since stable three-block β-alumina can be obtained in the absence of additives [21].

5.3. Effect of additives on densification

Many dopants do not either increase the concentration of mobile sodium ions or increase their mobility by altering the structure around them, rather they affect the degree of densification obtainable.

Yttria [75, 76] and titania [77] both appear to reside in the grain boundaries rather than in the bulk material, and cause the grain boundary resistance to decrease, thus increasing the overall conductivity of polycrystalline samples.

May [78] examined the influence of Ba^{2+} and Ti^{4+} and found that they were effective in stabilizing the β phase. From the corresponding increases in the lattice constants he determined that the Ti^{4+} entered the spinel block, replacing Al^{3+} ions, and Ba^{2+} replaced the Na^+ ions in the conduction plane. The result was an $\sim 65\%$ increase in resistivity and an $\sim 30\%$ increase in activation energy at ~ 573 K. The increase in resistivity was consistent with the increased fraction of β phase; however

this latter only partially explained the increased activation energy which was also believed to be the result of the blocking of the conduction plane by the large Ba^{2+} ions.

Calcium oxide has been found to have detrimental effects on the conductivity. Roth *et al.* [76] found that unlike magnesia, calcia resides in the conduction plane instead of in the spinel blocks. It thus effectively blocks the passage of Na^+ ions rather than increasing their concentration. This should lead to linear increase in resistivity with increasing concentration added; however, Buechele and De Jonghe [79] have shown that the exponential increase in resistivity with linearly increasing calcia doping level is due to calcium accumulating in the grain boundary region, forming $CaO{\cdot}6Al_2O_3$.

Wynn Jones and Miles [80] found that one per cent additions of titanium, zirconium, calcium and strontium enhanced sintering, permitting densification with lower firing temperatures (below 1750° C). They considered that the former two additives (Ti^{4+} and Zr^{4+}) substituted for Al^{3+} ions and thus caused Al^{3+} vacancies to be introduced in the spinel block as charge compensators. This allowed greater diffusion of the Al^{3+} ion which is the rate controlling step in the solid state sintering process. Thus densification could proceed without the presence of any secondary phase material preventing conductive contacts between the β-alumina grains.

The Ca^{2+} and Sr^{2+} additives, however, reduced the electrolytic conductivity, despite providing greater densification. Sintering may have occurred via an intermediate phase containing the calcium and strontium which was liquid and active at the firing temperatures (thereby increasing sintering rate), but inert at the lower temperatures relevant to its use as a solid electrolyte (thus decreasing the conductivity). Also, any substitution of Ca^{2+} or Sr^{2+} for Na^+ in the conduction planes would also decrease the conductivity by a blocking effect, owing to their large size.

Both SiO_2 and B_2O_3 are also additions to β-alumina which aid sintering [81] and therefore can be used to increase conductivity by achieving greater densification. However, Hsieh and De Jonghe [82] have shown that in large quantities (> 0.5 wt %) silica forms glassy sodium aluminosilicate phases which are inhomogeneously distributed. The glassy phase collected preferentially at triple grain junctions, but occasionally penetrated along some grain boundaries as a 1.0 to 2.0 nm thick layer. The presence of this silicate phase increased the resistivity of the grain boundaries. However, the effect was reduced when the sample was fired in soda-rich conditions, since the silicate phase increased the Na_2O content from its surroundings and hence increased its conductivity.

6. Production of β-alumina

6.1. Single crystal production

There are considerable difficulites associated with the single crystal growth of sodium β-alumina; for example, (i) the fact that β-alumina appears to decompose peritectically [23, 26], and (ii) the high vapour pressure of sodium over β-alumina at its decomposition temperature [23]. Cocks and Stormont [83] made use of an edge-defined, film-fed growth method (EFG) to counter these problems. This crystal growth method enables a variety of crystals to be grown having any constant cross-sectional shape. In the case of tubular crystal the liquid melt rises by capillary action to fill the feeding orifice in the tubular die [84–86]. A seed crystal is then brought into contact with the melt at the top of the capillary feed slot. After adjustment of the melt temperature and seed withdrawal rate, the melt spreads across the top surface of the die until further spreading is prevented by the 90° change in contact angle at both the inner and outer edges of the die. A tube begins to grow from the thin meniscus as the seed crystal is withdrawn.

To counter the problem of sodium vaporization, a high pressure (300 psi = 2.1 MN m^{-2}) inert gas, EFG crystal growth chamber was constructed, and to contain the reactive melt, both the crucible and the crystal-shaping dies were fabricated from iridium.

Even though a single β-alumina crystal was used as a seed in every case, none of the tubes whose β-alumina content was less than 100% was found to be a single crystal. In each case these tubes shared a two-phase alumina–β-alumina structure indicating a deficiency of Na_2O. To overcome this and achieve both a 100% β-alumina composition and also single crystal tubes it was found necessary to use melts containing an enriched concentration of Na_2O.

The exact composition of β-alumina is uncertain. For example, Weber and Venero [87] reported the composition as 10 to 12.2 mol % Na_2O and the incongruent melting point as 2240 ± 6 K, whereas Harata [88] suggested the range 10.9 to

13.7 mol % Na_2O. Cocks and Stormont [83] found that an initial composition of 20 mol % Na_2O was required to ensure a 100% β-alumina tube. Morrison *et al.* [89] continued this work and also investigated compositions containing magnesia. They produced tubes and ribbons of both β-alumina, magnesium-substituted β-alumina and β″-alumina grown in both the *a*- and *c*-axis directions at speeds of the order of mm h^{-1}.

The pseudo-binary diagram shown in Fig. 16 revealed that the use of Na_2O-enriched melts permitted growth of β-alumina via a flux method at temperatures below the peritectic decomposition temperature. During EFG growth the excess Na_2O concentration at the meniscus increased continually. However, Na_2O also evaporated from the meniscus, and equilibrium occurred at growth rates of ~3 to 9 mm h^{-1}.

At higher speeds, both monocrystallinity and single-phase structure were lost. At lower speeds single-crystal, single-phase β-alumina and magnesium-substituted β-alumina were grown, but not β″-alumina. The crystals produced were not optically clear because surface films, either enriched or depleted in Na_2O, developed.

6.2. Polycrystalline production—fabrication

There are a variety of different production routes for ceramic β-alumina. In the majority of cases the β-alumina is formed by calcination of precursor materials, typically sodium carbonate and β-alumina, at ~1260° C for ~2 h. The introduction of any additives is usually made at this stage. An example is the very effective method of introducing lithia discovered by Youngblood *et al.* [55]. This consists of forming ζ-lithium aluminate ($Li_2O \cdot 5Al_2O_3$) by mixing dried $LiNO_3$ and α-alumina and calcining at 1250° C for 2 to 3 h. The ζ-lithium aluminate can then be added in the required amounts to the sodium carbonate and α-alumina. The result is a "green" powder with a very even distribution of lithia.

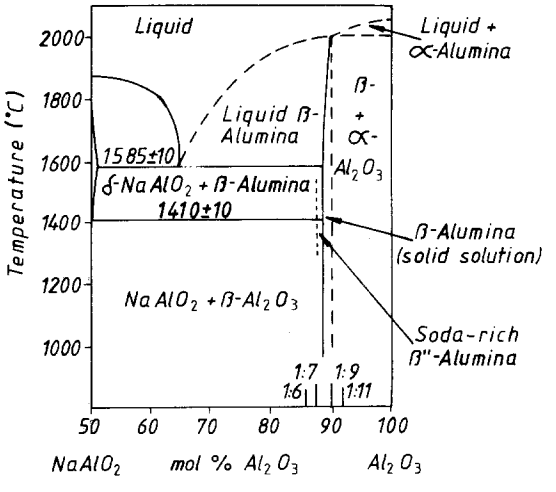

Figure 16 Section of Na_2O–Al_2O_3 pseudo-binary diagram containing Naβ- and Naβ″-alumina.

In the majority of cases the β-alumina is subsequently milled to produce a fine powder. Johnson *et al.* [90] have shown that it is possible to spray dry the β-aluminas using water-based slurries and to form a powder suitable for isostatic pressing. To avoid leaching of alkali from the calcined powders a second spray drying route was developed in which α-alumina was mixed with water-soluble alkalies and spray dried directly. This procedure had the advantage of eliminating the calcination and milling steps of the former process.

A variety of soluble alkali sources were used and in some cases a pre-burnout of the spray-dried powder pressing was necessary to prevent cracking of the tube during the initial stages of firing when the alkali salts dehydrated or decomposed. The most promising sources of alkali were considered to be the acetates and formates.

Vogel *et al.* [91] performed a similar investigation to Johnson *et al.* [90] and following thermoanalysis, thermogravimetric and dilatometric results, were able to propose several potential mechanisms to explain the 4% expansion of the acetate-based compacts during heat treatments up to 1200° C.

Once produced, the "green" powder can then be fabricated into the form of a closed-end tube. This tube can be formed by a variety of methods, including isostatic pressing, extrusion, slip casting and electrophoretic deposition.

6.2.1. Isostatic pressing

The important factors [92] in isostatic pressing are (i) powder flowability, (ii) powder packing (and compaction), and (iii) pressing pressure. For automated isostatic pressing (dry or wet bag), it is essential that flowable and fillable powders are available so that rapid bag filling (20 to 30 sec), reasonably low compaction ratios, and high green densities can be achieved.

Miller *et al.* [92] found that green density was fairly sensitive to pressing pressure, but, with some powders, the sintered density could be independent of it. Wynn Jones and Miles [80] used iso-

static pressing at pressures of 210 MN m^{-2} (30 000 psi) to form tubes of 16 mm outside diameter and 13 mm internal diameter, and up to 500 mm in length.

6.2.2. Extrusion

In an attempt to increase the production rate of β-alumina tubes over an isostatic pressing route, the Ford Motor Company developed an extrusion apparatus [93] which consisted of a fixed mandrel over which a moveable die was pushed, compressing powder between the two components. Powder compositions comprising > 80 wt % Al_2O_3 and 5 to 15 wt % Na_2O were thus extruded using a polyvinyl pyrrolidene–ethylene glycol binder at rates of 0.6 to 1.2 cm min^{-1}. Using an extrusion pressure of between 8 to 40 000 psi a greeen density of 45 to 60% of theoretical for a polycrystalline β″-alumina ceramic was achieved. Evaporation of the solvent and subsequent burning off of the binder in the tubes took place prior to sintering "in accordance with conventional techniques (e.g. 1585 to 1610° C)" which yielded bodies of between ~ 95 and 98% of theoretical density.

6.2.3. Slip casting

Bychalo *et al.* [94] slip cast β-alumina using aqueous suspensions with additives in plaster moulds. High density "green" ceramic was produced (~ 97% theoretical green density); however this was achieved by the capillary suction action of the mould aligning the plate-like β-alumina particles parallel to the mould walls. The packing of the platelets was thus highly efficient but the texture directionality was entirely wrong from the viewpoint of a high conductivity across the slip cast wall, owing to the high anisotropy of β-alumina.

Rivier and Pelton [95] have also slip cast β-alumina but using an entirely different technique. Rather than using conventional plaster moulds, which often result in sticking between mould and cast (especially true for long tubes which have a large surface area) and which must be replaced after about 5 castings as the pores become plugged, they used a powder casting method. The mould consisted of a powder of composition and mean particle diameter similar to that of the material being cast. The mean particle diameter had to be large enough so that the powder could be compacted to give a rigid mould but small enough to prevent passage of the suspension.

The mould was made of α-alumina powder (mean diameter of 4 μm) compacted around a glass tube. After removal of the tube, casting proceeded in normal fashion, using a methanol based slip. The advantages of this method were that after drying the cast could be removed very simply from the mould and the powder could be reused indefinitely after being dried. The range of dimensions capable of being formed are compatible with isostatic pressing. However, although microscopic examination of the slip-cast tubes indicated no evident texturing, anisotropy in sodium ion conduction could not be discounted.

6.2.4. Electrophoretic deposition

The electrophoretic forming operation is comprised of three main steps:

1. the preparation of a suitable suspension of powder dispersed in a vehicle, i.e. organic liquid;
2. the deposition of the powder from the suspension onto a mandrel using an electric field;
3. removal of the "green" compact from the mandrel.

There are several problem areas associated with this forming route, principally with the first of the three steps listed above.

Powers [96] has suggested that there are two competing charging modes with β-alumina. Negative charging, the predominant mode used by Powers, arising from dissociation of Na^+ ions from the particles, and positively charged particles obtained by adsorption of protons from water or organic acids such as stearic or benzoic acids. Thus a suitable charge was mainly achieved by control of the water content in the suspension.

Kennedy and Foissy [97], using dichloromethane as the deposition vehicle, found that they obtained both positive and negatively charged particles. The presence of small quantities of acid (especially trichloroacetic) stabilized the suspension and produced a better deposit, yet the particles were negatively charged. By the charging mechanisms suggested by Powers [96] the presence of acid should result in positively charged particles.

With negative charging Powers found that the vehicle in which the β-alumina particles were suspended must have a dielectric constant in the range 12 to 25 to achieve deposition. Such a liquid was found in n-amyl alcohol, which also resulted in a firm "green" compact and is relatively non-toxic.

Kennedy and Foissy have since investigated the mechanism of charge-production on suspended β-alumina particles [98]. Their conclusions were that simple models involving gain or loss of ions from the β-alumina particles were unlikely to be correct as they did not consider the effect of ions in the associated Stern layer of each particle. The net charge existing would be the result of competition among all cations and anions in the system, and thus the optimum conditons for deposition would depend upon the solvent system chosen.

Powers [96] noted that independent of the choice of solvent, if a number of depositions were carried out successively from the same suspension, then even though the voltage and time were kept constant, there was a gradual drop in the yield obtained owing to the decrease in concentration of the β-alumina. The remedy was found to be a steady increase in the deposition time, such that the product of concentration and time, $C \times t$, remained a constant.

Removal of the deposit from the mandrel required it to be slightly tapered, and for the deposition medium to be extracted, either by air-drying or by accelerated drying in a vacuum oven.

Once these conditions were satisfied then electrophoretic deposition was found to be a suitable method of forming β-alumina tubes. The conductivity results on such tubes, obtained by Kennedy and Foissy [97], were in good agreement with those for more standard sintered pellets, although the presence of dopants in the suspension appeared to have had little effect on the conductivity of the sintered product. This suggests that they did not deposit with the β-alumina.

6.3. Polycrystalline production – sintering

The first two of the production routes described above result in the tube formed requiring a preliminary bisque fire usually at 700 to 800° C to burn out any binders used. The tube is then sintered. Since soda volatilizes at elevated temperatures (>~1100° C), some method of preventing this must be employed. There are three principal methods of achieving this:

1. encapsulation in platinum containers;
2. encapsulation by a β-alumina buffer (either prefired tubing or powder);
3. zone sintering.

The first two methods result in a soda-rich atmosphere and thus reduce soda loss on firing. The third method, zone sintering, shows promise for commercial production of tubes, as it avoids a large capital outlay for platinum and it lends itself easily to continuous production.

6.3.1. Zone sintering

Zone sintering was developed for the rapid firing of β-alumina tubes by Wynn Jones and Miles [80] at the Electricity Council Research Centre (Capenhurst). The process allows precise control of the chemical composition of β-alumina and of the microstructure of the fired ceramic.

A zone sintering furnace consists of a graphite susceptor, with two α-Al_2O_3 tubes slotted through, heated by a 40 kW radio frequency (rf) generator operating at ~375 kHz. The larger tube is used for firing the β-alumina tubes, whilst the smaller tube is used for control purposes. The furnace temperature is controlled to ± 5 K by a closed loop system consisting of a radiation pyrometer interfaced with the r.f. generator, sensing the temperature of a small α-Al_2O_3 crucible in the centre of the control tube. The β-alumina tubes are fired in an α-alumina tube which is capable of being rotated at varying speeds inside the larger α-alumina tube mentioned above. This rotation counteracts the natural tendency of the tube to sag under gravity in the hot zone. The whole furnace assembly is sloped at 7.5° to the horizontal. This induces a natural convective air flow through the work tube maintaining a dynamic soda-rich atmosphere. It also prevents the residual moisture driven off the tubes in the hot zone from recondensing on the "green" tubes, which if it occurs leads to a rapid deterioration in the sintered bodies.

The "green" tubes are fed into the furnace at

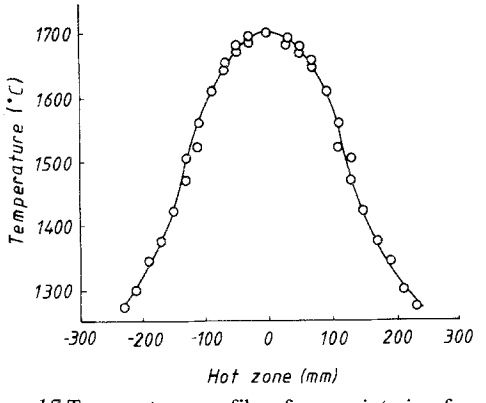

Figure 17 Temperature profile of zone-sintering furnace for β-alumina tubes.

the lower end at a constant rate by a conveyor system and they push each other through the furnace to the upper end where they enter a glass tube to minimize thermal shock. The temperature profile of the furnace is shown in Fig. 17. At high sintering speeds, densification can be incomplete and at low sintering speeds rapid grain growth occurs, resulting in trapped porosity. The relatively high vapour pressure of Na_2O also tends to inhibit densification at low sintering speeds as a high gas pressure inside a pore counteracts the normal driving force for sintering, i.e. a reduction in interfacial area. The optimum conditions are very sensitive to temperature and a 10° C change can result in a difference of 5 to 10% in the sintering speed for maximum density.

Wynn Jones and Miles [80] used the furnace at temperatures between 1600 and 1900° C, the samples passing through at a rate of $\sim 13\,mm\,min^{-1}$, which is equivalent to a 5 min firing with the length of the hot zone being about 64 mm. The effective heating rate was approximately $100°\,C\,min^{-1}$.

Powers and Mitoff [99] performed experiments using a horizontal tube furnace which had an approximately parabolic temperature profile (maximum temperature for 18 cm) to determine the effect of furnace atmosphere on sintering. They worked with dry and wet oxygen and air and found that moisture has little effect, unlike the presence of nitrogen. It appears to enter the pores and if the temperature rises high enough for these pores to become closed ($\sim 1750°$ C) then the N_2 becomes trapped and densification is reduced.

Such findings supported the belief that the densification process occurs by the formation of a transient liquid phase [100]. The reaction to form β- and β''-alumina takes place at $\sim 1600°$ C, corresponding closely with the eutectic temperature (1585° C) and both the rapid conversion and rate of densification would be explained by the existence of a liquid phase. It is also suggested by De Jonghe and Chandon [100] that addition of a small amount of the $NaAlO_2$–Al_2O_3 eutectic (melting point 1585° C) to a β-alumina powder allows densification at lower temperatures ($<1700°$ C), owing to the explicit use of a liquid phase. Such a reduction in the firing temperature significantly reduces grain growth. The eutectic composition was formed by the rapid decomposition of sodium and aluminium nitrates at 800° C for ~30 min in air.

6.3.2. Hot-pressing

In addition to a low resistance to sodium ion conduction, a high strength is required of β-alumina components. One method of achieving this is by the formation of fine grain sized ceramics. However, until the development of the zone-sintering technique previously described, it was not possible to achieve this criterion and maintain high conductivity by conventional pressureless sintering.

In 1974 Virkar *et al.* [101] reported their early attempts to use hot pressing using the lithia-stabilized β''-alumina composition. They achieved conductivities comparable to those reported for pressureless sintered β''-alumina [58], however the strength and fracture toughness were approximately doubled as a result of the higher densities (~ 100%) and finer grain size achieved. They used vacuum hot-pressing at temperatures of 1400° C in graphite dies and a pressure of $31\,MN\,m^{-2}$. These conditions resulted in incomplete phase conversion from β to β'' and so an extra annealing schedule of 24 h at 1400° C was required to obtain 100% β''-alumina. Further studies [102] revealed that powders already fully converted to β''-alumina before hot-pressing needed higher temperatures to achieve complete densification; thus it was concluded that densification kinetics were much faster than phase conversion.

McDonough *et al.* [103] hot-pressed commercial β-alumina powders in graphite dies at temperatures of 1500 to 1600° C and with pressures of $35\,MN\,m^{-2}$. They achieved ~ 100% dense samples with fine grain sizes (~ 5 μm) having a composition nearer to β than β''-alumina on account of the lack of a stabilizing additive. The resistivity, ρ, and strength, σ_f, were comparable with those of Virkar *et al.* [102] ($\rho = 3$ to $5\,\Omega\,cm$, $\sigma_f > 200\,MN\,m^{-2}$).

It was discovered [103] that the presence of silica was detrimental, resulting in poor final density and partial transformation to α-Al_2O_3. Moisture, similarly, resulted in increased transformation to α-Al_2O_3, even in powders stored in a manner designed to minimize moisture pick up. MgO additives were made to some of the powders used and an improvement in densification and thus strength was noted. This also occurred with additives of NaF and LiF. However, unlike the magnesia the fluorides resulted in a very large increase in the resistivity of the hot-pressed body. The fluoride additives appeared to inhibit the sodium conduction mechanism and hence negated the beneficial fabrication effect of

lowering the hot-pressing temperature from 1600° C to 1350° C.

The magnesia addition caused a slight decrease in resistivity although no β''-phase was detected. It was thought that limited quantities (below the detection limits of X-ray diffraction) of β''-alumina could have been formed which resided in the grain boundaries, thus decreasing the intergranular resistivity [103].

One disadvantage of hot-pressing is that the morphology of the β-alumina crystals caused texturing to occur. Both Virkar *et al.* [102] and McDonough *et al.* [103] have reported the existence of this phenomenon. The former reported resistivities perpendicular to the hot-pressing axis of between 1.4 to 1.8 times lower than parallel to the axis. Similar results for resistivity were reported by McDonough *et al.* [103] although the mechanical properties were not affected to any great degree.

One advantage afforded by hot-pressing is that it enables densification mechanisms to be determined. The use of pressure as a variable during studies of sintering is valuable in two ways:

1. It indirectly reduces the interference from such processes as grain growth and surface diffusion; and

2. It directly distinguishes between mechanisms with different pressure dependence.

Hind and Roberts [104] used hot-pressing (in addition to fast firing) to study the sintering and densification kinetics of β-alumina. The phase diagram proposed by Rolin and Thanh [25] includes a eutectic point at 1410° C for a composition containing 55 mol% Al_2O_3; β''-alumina (84 mol% Al_2O_3, 16 mol% Na_2O) sintered at this temperature would contain about 8 mol% liquid.

De Vries and Roth [26] questioned the existence of this eutectic and assigned that area of the diagram to an assumed new polymorph δ. The fast-firing data obtained by Hind and Roberts [104] confirmed that the phase composition–temperature relationships suggested by De Vries and Roth were essentially correct for the high-alumina compositions. However, to determine the densification kinetics of the high soda content $Na_2O \cdot 5Al_2O_3$ hot pressing had to be used. Any change in the creep mechanism can be detected from the stress dependence across a temperature range. Thus Hind and Roberts examined the relationships between the applied stress and the densification rate at 1375 and 1475° C. They discovered a change from a dislocation creep to a diffusional creep controlled densification mechanism, which supports the existence of a eutectic at 1410° C for the composition $Na_2O \cdot 5Al_2O_3$ as suggested by Rolin and Thank [25].

6.3.3. Plasma sintering

An induction-coupled plasma [105] was used to sinter tubes of lithia-stabilized β''-alumina in static and flowing argon atmospheres. The former atmosphere was found to result in a lower degree of soda loss, presumably as a result of a build-up of a sodium oxide partial pressure. Matrix grain sizes in the range of 5 to 10 μm could be obtained but exaggerated grain growth was always found near the exterior wall. Soda loss was ~10% from the bulk, rising to ~15% for the outer 100 μm of the tube surface. Another disadvantage with this sintering route was that the degree of conversion to the β''-phase varied throughout the structure. Thus while the central portion exhibited essentially 100% conversion, the closed-end tip of the tubes varied from ~33 to 55% conversion, depending on the starting powder. This method appears to be less successful than either zone or conventional pressureless sintering routes.

7. Conclusions

The crystal structures of both β- and β''-alumina have been accurately described and used to explain the phenomenon of Na^+ ion transport in these unusual materials. However, the phase diagram of the $NaAlO_2$–Al_2O_3 system, partly established, requires further investigation since considerable differences are still to be found in the literature. The discrepancies are thought to arise from the range of compositions over which the β-aluminas are capable of existing, the experimental techniques and possibly even the starting materials. Such uncertainties as remain are largely academic, however, since the majority of commercial applications for the β-aluminas involve addition of the β''-alumina stabilizing agents, magnesia and lithia, with the result that the determination of the ternary phase diagrams is of considerable practical importance.

Values for both the polycrystalline and single crystal ionic conductivity of the β-aluminas show a wide distribution. This is due not only to the variation in composition but also to the diverse techniques by which conductivity has been measured. Several groups have proposed increas-

ingly sophisticated mechanisms for the conduction mechanism; however differences between practical results and theory are still present, indicating a need for further refinement of the theories.

The effect of impurity ions on the physical properties of the β-aluminas has largely been measured and accounted for; any further work is therefore likely to be concerned with specific applications rather than a general investigation.

Much of the current research on β-alumina is concerned with optimizing fabrication techniques and physical and mechanical properties. Single crystal production has been investigated with a substantial degree of success, the conditions leading to a uniform composition throughout the crystal having been determined. For polycrystalline electrolyte the advent of water based spray-drying powder production has had a significant impact in that the time required to produce a green body has been considerably reduced, although it has complicated the sintering schedule by necessitating a pre-fire.

β-alumina green bodies have been formed by isostatic pressing, extrusion, slip casting and electrophoretic deposition. A problem common to all these techniques arises due to the anisotropy of the β-alumina crystals; this can result in adverse texturing and thus reduction of the conductivity across a membrane wall. With the possible exception of slip casting, techniques to overcome this problem appear to have been found.

The sintering of β-alumina has always been accompanied by soda loss; however the presence of a soda-rich atmosphere (generated by either encapsulation in platinum, by use of a β-alumina buffer or by rapid firing, e.g. zone sintering) has been found to alleviate the problem. Following extensive development zone sintering has now reached the preproduction stage where consistent quality electrolyte can be manufactured.

The properties of the β-aluminas of commercial potential have thus been extensively explored. Research investigations are still underway, but it would appear that it is the fabrication technology of these fast ion transport materials that presents the major challenge of the future.

References

1. D. A. J. RAND, *J. Power Sources* **4** (1979) 101.
2. N. WEBER and J. T. KUMMER, Advances in Energy Conversion Engineering ASME Conference, Florida, 1967, p. 913.
3. J. N. ANAND, in *Proc. Intersoc. Energy Conv. Conf.* **14** (1979) 698.
4. H. Y-P. HONG, *Mater. Res. Bull.* **11** (1876) 173.
5. J. B. GOODENOUGH, H. Y-P. HONG and J. A. KAFALAS, *ibid.* **11** (1976) 203.
6. G. A. RANKIN and H. E. MERWIN, *J. Amer. Chem. Soc.* **38** (1916) 568.
7. C. W. STILLWELL, *J. Phys. Chem.* **30** [11] (1926) 1441.
8. W. L. BRAGG, C. GOTTFRIED and J. WEST, *Z. Krist.* **77** [3–4] (1931) 255.
9. G. C. FARRINGTON and J. L. BRIANT, *Mater. Res. Bull.* **13** (1978) 763.
10. R. RIDGWAY, A. KLEIN and W. O'LEARY, *Trans. Electrochem. Soc.* **70** (1836) 71.
11. C. A. BEEVERS and S. BROHULT, *Z. Krist.* **95** (1936) 472.
12. C. A. BEEVERS and M. A. S. ROSS, *ibid.* **97** (1937) 59.
13. J. FELSCHE, *ibid.* **127** (1968) 94.
14. C. R. PETERS, M. BETTMAN, J. W. MOORE and M. D. GLICK, *Acta Crystall.* **B27** (1971) 1826.
15. Y. F. YAO and J. T. KUMMER, *J. Inorg. Nucl. Chem.* **29** (1967) 2453.
16. W. L. ROTH, F. REIDINGER and S. LA PLACA, in "Superionic Conductors", edited by G. D. Mahan and W. L. Roth (Plenum Press, New York, 1976) p. 223.
17. R. R. DUBIN, H. S. STORY, R. W. POWERS and W. C. BAILEY, *Mater. Res. Bull.* **14** (1979) 185.
18. M. W. BREITER and G. C. FARRINGTON, *ibid.* **13** (1978) 1213.
19. G. YAMAGUCHI, *Elect. Chem. Soc. Japan* **11** (1943) 260.
20. J. THERY and D. BRIANCON, *Comptes Rendus. hebd. Seanc. Acad. Sci. Paris* **254** (1962) 2782.
21. *Idem, Rev. Hautes Temper. Refract.* **1** (1964) 221.
22. G. YAMAGUCHI and K. SUZUKI, *Bull. Chem. Soc. Japan* **41** (1968) 93.
23. J. T. KUMMER, *Prog. Solid State Chem.* **7** (1972) 141.
24. M. BETTMAN and L. L. TURNER, *Inorg. Chem.* **10** (1971) 1442.
25. M. ROLIN and P. H. THANH, *Rev. Hautes Temper. Refract.* **2** (1965) 175.
26. R. C. DE VRIES and W. L. ROTH, *J. Amer. Ceram. Soc.* **52** (1969) 364.
27. J. LIEBERTZ, *Ber. Dt. Keram. Ges.* **49** (1972) 288.
28. Y. LE CARS, J. THERY and R. COLLONGUES, *Rev. Hautes Temper. Refract.* **9** (1972) 153.
29. *Idem, Comptes Rendus. Acad. Sci. Paris.* **C274** (1972) 4.
30. J. D. BEVAN, B. HUDSON and P. T. MOSELY, *Mater. Res. Bull.* **9** (1974) 1073.
31. I. IMAI and M. HARATA, *Jpn. J. Appl. Phys.* **11** (1972) 180.
32. N. WEBER and A. F. VENERO, in Proceedings of the 72nd Annual Meeting of The American Ceramic Society, Philadelphia, PA., May 1970, (Joint Session V No. 1-JV-70) [Ceram. Bull. **49** (1970) 498.]
33. Research on Electrodes and Electrolyte for the Ford Sodium–Sulphur Battery; Report Contract No. NSF-C805 (a) July 1974, (b) January 1976.

34. H. SAALFIELD, *Naturwiss.* **43** (1956) 420.
35. J. H. KENNEDY, "Solid Electrolytes", Topics in Applied Physics Vol. 21, edited by S. Geller (1977) Ch. 5.
36. R. H. RADZILOWSKI, Y. F. YAO and J. T. KUMMER, *J. Appl. Phys.* **40** (1969) 4716.
37. B. J. DUNBAR and S. SARIAN, in Proceedings of the American Ceramic Society 28th Pacific Coast Regional and Nuclear Div. Meeting, October 29–31 (1975) 4-FC-75P.
38. D. S. DEMMOTT and P. HANCOCK, *Proc. Brit. Ceram. Soc.* **19** (1971) 193.
39. A. HOOPER, *J. Phys. D. Appl. Phys.* **10** (1977) 1487.
40. M. S. WHITTINGHAM and R. A. HUGGINS, *J. Chem. Phys.* **54** (1971) 414.
41. R. M. DELL and P. T. MOSELY, *J. Power Sources* **6** (1981) 143.
42. M. A. M. BOURKE, A. HOOPER, P. T. MOSELY and R. G. TAYLOR, *Solid State Ionics (Netherlands)* **1** (1980) 367.
43. W. HAYES, L. HOLDEN and B. C. TOFIELD, *J. Phys. C (GB)* **14** (1981) 511.
44. Y. LE CARS, R. COMES, L. DESCHARGES and J. THERY, *Acta Crystall.* **A30** (1974) 305.
45. Ph. COLOMBAN and G. LUCAZEAU, *J. Chem. Phys.* **72** (1980) 1213.
46. M. S. WHITTINGHAM and R. A. HUGGINS, *J. Electrochem. Soc.* **118** (1971) 1.
47. W. KOCH and C. WAGNER, *Z. Phys. Chem.* **B38** (1937) 295.
48. J. C. WANG, M. GAFFARI and S. CHOI, *J. Chem. Phys.* **63** (1975) 772.
49. W. L. ROTH, *J. Solid State Chem.* **4** (1972) 60.
50. D. WOLF, *J. Phys. Chem. Solids* **40** (1979) 757.
51. D. B. M. WHAN, P. D. DERNIER, C. VETTIER, A. S. COOPER and J. P. REMEIKA, *Phys. Rev.* **B17** (1978) 4043.
52. K. K. KIM, J. N. MUNDY and W. K. CHEN, *J. Phys. Chem. Solids* **40** (1979) 757.
53. L. L. CHASE, C. H. HAO and G. D. MAHAN, *Solid State Commun.* **18** (1976) 401.
54. G. J. MAY, *J. Power Sources* **3** (1978) 1.
55. G. E. YOUNGBLOOD, A. V. VIRKAR, W. R. CANNON and R. S. GORDON, *Ceram. Bull.* **56** (1977) 206.
56. G. E. YOUNGBLOOD, G. R. MILLER and R. S. GORDON, *J. Amer. Ceram. Soc.* **61** (1978) 86.
57. L. J. MILES and R. STEVENS, private communication.
58. T. J. WHALEN, G. J. TENNENHOUSE and C. MEYER, *J. Amer. Ceram. Soc.* **57** (1974) 497.
59. A. V. VIRKAR, G. R. MILLER and R. S. GORDON, *ibid.* **61** (1978) 250.
60. T. OHTA, M. HARATA and A. IMAI, *Mater. Res. Bull.* **11** (1976) 1343.
61. G. E. YOUNGBLOOD and R. S. GORDON, *Ceramurgia Int.* **4** (1978) 93.
62. L. C. DE JONGHE, *J. Mater. Sci.* **11** (1976) 206.
63. R. STEVENS, *ibid.* **9** (1974) 801.
64. L. C. DE JONGHE, *ibid.* **10** (1975) 2173.
65. Y. LE CARS, D. GRATIAS, R. PORTIER and J. THERY, *J. Solid State Chem.* **15** (1975) 218.
66. L. C. DE JONGHE, *J. Amer. Ceram. Soc.* **62** [5–6] (1979) 289.
67. R. W. POWERS and S. P. MITOFF, *J. Electrochem. Soc.* **122** (1975) 226.
68. J. H. KENNEDY, in "Superionic Conductors", edited by G. D. Mahan and W. L. Roth (Plenum Press, New York, 1976) p. 335.
69. J. H. KENNEDY and A. F. SAMMELLS, *J. Electrochem. Soc.* **119** (1972) 1609.
70. J. H. KENNEDY and J. R. AKRIDGE, Electrochem. Soc. Meeting Paper 84, Washington D.C. May 2–7 1976.
71. J. P. BOILOT and J. THERY, *Mater. Res. Bull.* **11** (1976) 407.
72. W. G. BUGDEN and J. H. DUNCAN, *Sci. Ceram.* **9** (1977) 348.
73. R. H. RADZILOWSKI, *J. Amer. Ceram. Soc.* **53** (1970) 699.
74. B. C. TOFIELD and G. C. FARRINGTON, *Nature (London)* **278** (1979) 438.
75. R. J. CHARLES, S. P. MITOFF and W. G. MORRIS, U.S. Patent No. 3,607,435, Sept. 21, 1971.
76. W. L. ROTH, CHUNG INTAIK and H. S. STORY, *J. Amer. Ceram. Soc.* **60** (1977) 311.
77. K. NISHIMURA, M. HASEGAWA and M. TAHAGI, Japanese Patent No. 73-43, 646, Dec. 20 1973.
78. G. J. MAY, *J. Mater. Sci.* **14** (1979) 1502.
79. A. C. BUECHELE and L. C. DE JONGHE, *Ceram. Bull.* **58** (1979) 861.
80. I. WYNN JONES and L. J. MILES, *Proc. Brit. Ceram. Soc.* **19** (1971) 161.
81. J. T. KUMMER and N. WEBER, U.S. Patent No. 3,404,036, Oct. 1, 1968.
82. M. Y. HSIEH and L. C. DE JONGHE, *J. Amer. Ceram. Soc.* **61** (1976) 185.
83. F. H. COCKS and R. W. STORMONT, *J. Electrochem. Soc.* **121** (1974) 596.
84. H. E. LA BELLE, Jr and A. I. MLAUSKY, *Mater. Res. Bull.* **6** (1971) 571.
85. B. CHALMERS, H. E. LA BELLE Jr and A. I. MLAUSKY, *ibid.* **6** (1971) 681.
86. H. E. LA BELLE Jr, *ibid.* **6** (1971) 581.
87. N. WEBER and A. F. VENERO, Proceedings of the 72nd Annual Meeting of The American Ceramic Society Philadelphia PA. May 5 1970 (Joint Session I No. 5-JI-70).
88. M. HARATA, *Mater. Res. Bull.* **6** (1971) 461.
89. A. D. MORRISON, R. W. STORMONT and F. H. COCKS, *J. Amer. Ceram. Soc.* **58** (1975) 41.
90. D. W. JOHNSON, Jr, S. M. GRANSTAFF, Jr and W. W. RHODES, *Ceram. Bull.* **58** (1979) 849.
91. E. M. VOGEL, J. W. JOHNSON, Jr and M. F. YAN, *ibid.* **60** (1981) 494.
92. M. L. MILLER, B. J. McENTIRE, G. R. MILLER and R. S. GORDON, *ibid.* **58** (1979) 522.
93. Ford Motor Company, U.K. Patent No. 1,541,850 (1979).
94. W. BYCHALO, G. ROSENBLATT, J. LAM and P. S. NICHOLSON, *Ceram. Bull.* **55** (1976) 286.
95. M. RIVIER and A. D. PELTON, *ibid.* **57** (1978) 183.

96. A. W. POWERS, *J. Electrochem Soc.* **122** (1975) 490.
97. J. H. KENNEDY and A. FOISSY, *ibid.* **122** (1975) 482.
98. *Idem, J. Amer. Ceram. Soc.* **60** (1977) 33.
99. R. W. POWERS and S. P. MITOFF, *Ceram. Bull.* **56** (1977) 456.
100. L. C. DE JONGHE and H. CHANDON, *ibid.* **55** (1976) 312.
101. A. V. VIRKAR, G. J. TENNENHOUSE and R. S. GORDON, *J. Amer. Ceram. Soc.* **57** (1974) 508.
102. A. V. VIRKAR, T. D. KETCHAM and R. S. GORDON, *Ceramurgia Int.* **5** (1979) 66.
103. W. J. MCDONOUGH, D. R. FLINN, K. H. STERN and R. W. RICE, *J. Mater. Sci.* **13** (1978) 2403.
104. D. HIND and E. W. ROBERTS, *Trans. J. Brit. Ceram. Soc.* **80** (1981) 219.
105. D. L. JOHNSON and R. A. RIZZO, *Ceram. Bull.* **59** (1980) 467.

Received 1 April
and accepted 26 April 1983